International Journal of Thermophysics, Vol. 15, No. 3, 1994

Measurement of Thermal Diffusivity and Anisotropy of Plasma-Sprayed Coatings

A.-S. Houlbert,[1,2] P. Cielo,[1] C. Moreau,[1] and M. Lamontagne[1]

Received November 1, 1993

The thermal diffusivity of free-standing tungsten and zirconia plasma-sprayed coatings was measured in the directions parallel and perpendicular to their surface. The parallel thermal diffusivity was evaluated by a double-sensing Laplace-transform technique and compared to the perpendicular values obtained by the flash technique. Ratios between the parallel and the perpendicular thermal diffusivity values were in the range of 1.1 to 1.5 for zirconia and 4 to 6 for tungsten. The results are discussed in terms of the coating thickness and microstructure.

KEY WORDS: coatings; plasma-spray; thermal anisotropy; thermal diffusivity; tungsten; zirconia.

1. INTRODUCTION

Directional thermal properties of plasma-sprayed coatings are important both because of their correlation with the coating microstructure [1–3] and because they often affect perpendicular thermal diffusivity measurements [4, 5].

Thermal properties of plasma-sprayed coatings, usually in the direction perpendicular to the surface, have been investigated by a number of authors [3–19]. The layered microstructure of plasma-sprayed coatings and the observation of perpendicular thermal diffusivity values which are typically 2 to 20 times smaller than the thermal diffusivity of the same materials in a well-compacted state suggest a high degree of thermal anisotropy in plasma-sprayed coatings. Recent measurements [20] on metallic and ceramic coatings provided, however, relatively low thermal

[1] National Research Council of Canada, Industrial Materials Institute, 75 Boul. de Mortagne, Boucherville, Québec J4B 6Y4, Canada.

[2] On leave from Laboratoire d'Énergetique et de Méchanique Théorique et Appliquée, B.P. 160, 54504 Vandoeuvre les Nancy, France.

0195-928X/94/0500-0525$07.00/0

anisotropy values, in the range of 0.8 to 2, if the measured values of the parallel and perpendicular thermal diffusivity are compared.

A variety of techniques is available for the measurement of the thermal diffusivity in a direction either parallel or perpendicular to the sample surface [21, 22]. A method using a laterally confined heating source on the sample front and two radially separated thermocouples was initially developed by Donaldson and Taylor [23–25]. This approach is, however, convenient mostly with relatively thick samples. Spot-heating thermographic techniques [26, 27] are useful mainly for the determination of thermal anisotropy in the plane parallel to the sample surface; their extension to three-dimensional (3-D) thermal anisotropy evaluation [26] is affected by a number of experimental uncertainties, namely, by surface losses. Similar surface loss problems, particularly with thin samples, as well as focusing and alignment difficulties, are encountered with the converging-thermal wave method [28–30]. Similar considerations are valid for line-heating techniques [31]. Methods using a multiplicity of fine thermocouples precisely spaced with respect to the heater [32] are strongly affected by positioning uncertainties. A simpler approach was recently presented [33] where two thermocouples are spaced apart along a thin strip heated by a contact heater. In this case, one can minimize by proper data reduction the sensitivity to surface losses and obtain a good sensitivity to the thermal diffusivity over a wide range of Biot numbers.

This paper describes the measurement of the thermal diffusivity of free-standing tungsten and zirconia plasma-sprayed coatings in the directions parallel and perpendicular to the surface. For the perpendicular direction the classical flash technique is used. For the measurement of the parallel thermal diffusivity, a double-sensing method [33] was adopted, where the two thermocouples are replaced by a single, focused infrared detector, which is alternately positioned over the two sensing positons situated a few millimeters apart along the thin sample. By using a micrometric positioner, we could thus obtain a high precision in the sensor distance independently of the optics-limited sharpness of their focus, while avoiding thermal perturbations from contact thermocouples.

2. DESCRIPTION OF THE THERMAL MEASUREMENT METHODS

2.1. Thermal Diffusivity Measurement in the Direction Normal to the Surface by a Flash Technique

The well-known flash method relies on the generation of a thermal pulse on one face of a thin sample and on the observation of the temperature history on the opposite face.

The basic approach was originally proposed by Parker et al. [34] They assumed as the sample a perfectly insulated cylinder, receiving at $t=0$ a Dirac thermal pulse uniformly over one face. By solving the thermal equation for the temperature on the opposite face, one obtains for the thermal diffusivity

$$a = 0.139e^2/t_{1/2} \tag{1}$$

where e is the sample thickness and $t_{1/2}$ is the time period corresponding to a temperature rise to half of the maximum temperature at the back of the sample. This method is simple, but it is affected by the thermal losses over the sample faces. A number of procedures [35] are possible to account for the thermal losses. Most often, the surface loss coefficients are evaluated and an iterative approach leads to the value of the thermal diffusivity.

We have followed a variation of this technique developed by Degiovanni [35], which both is simple and does not require a previous evaluation of the loss coefficients. A homogeneous and in-plane isotropic cylindrical sample of thickness e and radius R is assumed with surface loss coefficients h_0, h_e, and h_R over its front, back, and lateral faces, respectively (Fig. 1). We assume that at $t=0$ its temperature distribution can be expressed as the product of a function of r and a function of z. The subsequent bidirectional heat propagation in the sample is calculated by separation of variables and the solution is obtained as a double series. The expression for the temperature at a point $r=r_c$ on the back face depends on the five parameters e/R, r_c/R, and the Biot numbers $h_R R/\lambda$, $h_0 e/\lambda$, and $h_e e/\lambda$, λ being the thermal conductivity of the sample material.

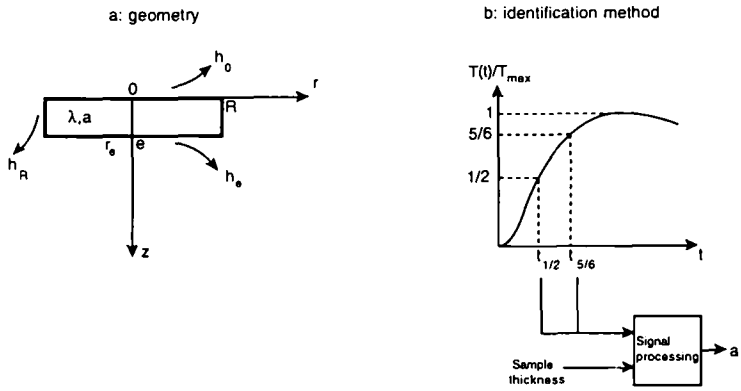

Fig. 1. Shematic diagram of the flash technique adopted in this work.

An intermediate time $t_{5/6}$ is defined as the time period corresponding to a temperature rise to five-sixths of the maximum temperature. The corresponding Fourier number is

$$t^*_{5/6} = at_{5/6}/e^2 \tag{2}$$

A curve of $t_{1/2}/t_{5/6} = f(t^*_{5/6})$ has been obtained by modeling for different values of $t^*_{5/6}$. It has been shown numerically [35] that such a curve is independent of the five parameters e/R, r_c/R, $h_R R/\lambda$, $h_0 e/\lambda$, and $h_c e/\lambda$ over a wide range of practical cases and can be approximated by the following expression:

$$t^*_{5/6} = 0.968 - 1.6382\left(\frac{t_{1/2}}{t_{5/6}}\right) + 0.6148\left(\frac{t_{1/2}}{t_{5/6}}\right)^2 \tag{3}$$

The procedure to obtain the thermal diffusivity is thus the following: The experimental temperature evolution curve is normalized and the values of $t_{1/2}$ and $t_{5/6}$ recorded. Equation (3) is then used to obtain $t^*_{5/6}$, and then Eq. (2) gives the thermal diffusivity a.

Other choices are possible for the intermediate time periods such as $t_{1/3}$ and $t_{2/3}$ with equivalent results. The reproducibility of the results has been shown by modeling to be within 0.5 and 3%. In our case, this method is used to evaluate the axial diffusivity of thin anisotropic samples. The approach is still applicable because the thermal pulse is uniformly injected over the full sample face, so that heat propagation is unidirectional.

2.2. Thermal Diffusivity Measurement in the Direction Parallel to the Surface by a Strip Monitoring Technique

2.2.1. Description of the Technique

We followed the approach recently developed by Hadisaroyo et al. [33] to evaluate the lateral thermal diffusivity of the plasma-sprayed coatings. The basic approach is the following (Fig. 2): A heat pulse is injected over one end of a strip. Temperature is monitored at two positions along the strip. Through signal processing, the thermal diffusivity along the strip and the Biot number are obtained. The overall procedure is now described.

As shown in Fig. 2, the sample is a strip of thickness e and length much larger than the thermal propagation during the measurement. Its face-normal thermal conductivity is $\lambda_\perp$, the thermal conductivity along the x axis is λ, and the volume heat capacity ρc. Heat losses with a coefficient h are assumed to be uniform over its upper and lower surfaces. The strip

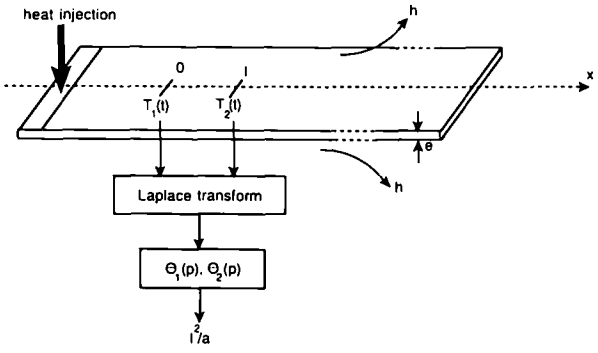

Fig. 2. Schematic diagram of the strip monitoring technique adopted in this work.

is thin enough so that the Biot number $\mathrm{Bi} = he/\lambda_\perp$ is smaller than unity. Heat propagation can thus be assumed to be unidirectional along the x direction, and the surface losses φ can be distributed through the volume, so that the temperature $T(x, t)$ monitored at time t in the position x follows the equation

$$\rho c \frac{\partial T(x, t)}{\partial t} = \lambda \frac{\partial^2 T(x, t)}{\partial x^2} + p(x, t) \tag{4}$$

where

$$p(x, t) = -\frac{\varphi}{S\,dx} = \frac{-hm\,dx[T(x, t) - T_e]}{S\,dx} \tag{5}$$

S being the strip cross section, m the perimeter of such a section, and T_e the temperature of the surrounding air. By introducing $T'(x, t) = T(x, t) - T_e$, the diffusivity $a = \lambda/\rho c$, and the approximation $m/S \cong 2/e$ for a thin strip, one obtains

$$\frac{\partial^2 T'}{\partial x^2} - \frac{2h}{\lambda e} T' = \frac{1}{a} \frac{\partial T'}{\partial t} \tag{6}$$

If we now introduce the boundary conditions requiring the strip temperature to be equal to the ambient temperature before heating, the temperature at $x = 0$ to follow a given expression $T_1(t)$, and the strip to be thermally long,

$$\begin{aligned} T'(x, 0) &= T(x, 0) - T_e = 0 \\ T'(0, t) &= T(0, t) - T_e = T_1(t) \\ T'(x, t) &= 0 \qquad \text{for} \quad x \to \infty \end{aligned} \tag{7}$$

and perform a Laplace transform, we obtain

$$\frac{\partial^2\theta}{\partial x^2}-\left(\frac{p}{a}+\frac{2h}{\lambda e}\right)\theta=0 \tag{8}$$

where p is the Laplace variable and $\theta(x, p)=\int_0^{\infty} T'(x, t)\exp(-pt)\,dt$.

By defining $\theta_1(p)=\theta(0, p)$ and $\theta_2(p)=\theta(l, p)$, we obtain from Eq. (8)

$$\frac{\theta_2(p)}{\theta_1(p)}=\exp\left[-\left(\frac{l^2}{a}p+\frac{2hl^2}{\lambda e}\right)^{0.5}\right] \tag{9}$$

or

$$\ln^2\left(\frac{\theta_2(p)}{\theta_1(p)}\right)=\frac{l^2}{a}p+\frac{2hl^2}{\lambda e} \tag{10}$$

The procedure for evaluating the thermal diffusivity is then the following: The Laplace transforms of the experimental curves $T_1(t)$ and $T_2(t)$ are computed, $\ln^2[\theta_2(p)/\theta_1(p)]$ is plotted vs p, and the slope gives l^2/a and thus a. It should be noted that Eq. (10) is independent of the actual shape of the injected heat pulse.

The practical limitations of this method are due to the finite duration of the recorded signal and to the limited signal/noise ratio at the beginning of the recording. In view of these limitations, we chose as the working interval [valid in the case of a temperature $T_2(t)$ decreasing at the end of the recording]

$$[p_{\min}, p_{\max}]=\left[\frac{6}{t_{\max}}, \frac{1}{t_{\min}}\right] \tag{11}$$

where $t_{\max}$ is the maximal duration of the temperature recording and $t_{\min}$ corresponds to a value of $T_2(t)$ equal to 5/100 of its maximum value.

2.2.2. Sensitivity to the Different Parameters

Ideally, this method should be unaffected by the level of the surface loss coefficient h. In practice, we now show that the sensitivity $Z_{h/\lambda}$ of the measurement to h/λ is usually much smaller than the sensitivity Z_a to the thermal diffusivity a. One obtains by differentiation

$$Z_a=a\frac{\partial[\theta_2(p)/\theta_1(p)]}{\partial a}=\frac{p^*}{2(p^*+2b)^{0.5}}\exp[-(p^*+2b)^{0.5}] \tag{12}$$

and

$$Z_{h/\lambda}=\frac{h}{\lambda}\frac{\partial(\theta_2(p)/\theta_1(p))}{\partial(h/\lambda)}=\frac{-b}{(p^*+2b)^{0.5}}\exp[-(p^*+2b)^{0.5}] \tag{13}$$

where $p^*=(l^2/a)\,p$ and $b=(hl/\lambda)(l/e)$.

In our case, the samples have a thickness $e \cong 1$ mm, a natural convection loss coefficient $h \cong 5\ \mathrm{W \cdot m^{-2} \cdot K^{-1}}$, and $\lambda \cong 1\ \mathrm{W \cdot m^{-1} \cdot K^{-1}}$ for zirconia and $10\ \mathrm{W \cdot m^{-1} \cdot K^{-1}}$ for tungsten. We thus obtain, for the zirconia coating,

$$b = 0.02 \quad \text{for} \quad l = 2\ \text{mm}$$

$$b = 0.125 \quad \text{for} \quad l = 5\ \text{mm}$$

For tungsten, one obtains

$$b = 0.0125 \quad \text{for} \quad l = 5\ \text{mm}$$

$$b = 0.05 \quad \text{for} \quad l = 10\ \text{mm}$$

Figure 3 shows the corresponding sensitivities to a and h/λ for $b = 0.002$ and $b = 0.1$. The curves are not strongly affected by the value of b. One can note that for short values of the time (large values of p^*), surface losses have little influence, while for longer times (small values of p^*) the effect of surface losses is more important. We have correspondingly chosen $p^* > 1$, or $p > (a/l^2)$ for our interval. We thus obtain, for zirconia ($a \cong 5 \times 10^{-7}\ \mathrm{m^2 \cdot s^{-1}}$),

$$p > 0.125 \quad \text{if} \quad l = 2\ \text{mm}$$

$$p > 0.02 \quad \text{if} \quad l = 5\ \text{mm}$$

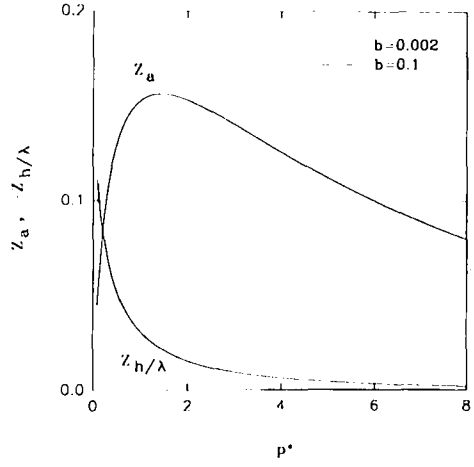

Fig. 3. Computed sensitivity coefficients for the strip monitoring method.

and, for tungsten ($a \cong 15 \times 10^{-6}$ m$^2 \cdot$s^{-1}),

$$p > 0.6 \quad \text{if} \quad l = 5 \text{ mm}$$

$$p > 0.15 \quad \text{if} \quad l = 10 \text{ mm}$$

It should be noted from the above considerations and from Eq. (11) that we must have $6/t_{max} > a/l^2$, or $t_{max} < 6l^2/a$. One must thus make sure that the heating time and the distance l between the monitored spots are compatible with each other.

3. DESCRIPTION OF THE SAMPLES

The samples were produced by plasma-spraying, in air, the coating over a copper substrate (copper thickness, 2.4 mm; previously sandblasted with 24-grit alumina under a pressure of 30 psig) and then eliminating the substrate.

The plasma-spraying torch was a Plasmadyne SG100, with a No. 129 cathode and a No. 145 anode, ejection gas No. 113. The power was 33.3 kW (900 A and 37 V). The arc gas was argon and the auxiliary gas helium (32% helium, with 50 L$\cdot$min^{-1} for argon and 23.6 L$\cdot$min^{-1} for helium). The standoff distance during projection, over a surface of 120×160 mm^2, was 76 mm. Spraying was carried out through suitable masks (either a 100- × 12-mm slit or circular holes of 10- and 20-mm diameter) to shape the sprayed area better. The substrate was cooled with a nitrogen jet, while the front surface was air-blasted to eliminate aerosols.

Zirconia coatings of nearly 0.8-mm thickness were obtained with zirconia–8% yttria powder of granulometry 22.5–45 μm; Amperit, 825.1; powder flow, 22 g$\cdot$min^{-1}; and powder-carrying argon gas flow, 6.6 L$\cdot$min^{-1}. The torch was laterally scanned at 0.5 m$\cdot$s^{-1}. Tungsten coatings of 0.8 and 1.3 mm were obtained under the same conditions, with 99.5% pure tungsten powder Metco NS61; granulometry, 30–74 μm; powder flow, 32 L$\cdot$min^{-1}; powder-carrying argon gas flow, 10.6 L$\cdot$min^{-1}; and torch scanning speed, 0.2 m$\cdot$s^{-1}.

The coating samples were subsequently separated from the substrate by chemical etching, during 2 h, in a 50% water solution of nitric acid, which does not substantially attack either zirconia or tungsten. We verified on similar samples that the mass of the sprayed deposits did not change after a 2-h immersion and that no significant oxidation took place, as observed by comparing the infrared transmission spectra of zirconia before and after immersion. The thickness fluctuations over the disk-shaped samples were of the order of the surface roughness, 10 μm. Thickness fluctuations over the longer, strip-shaped samples were slightly higher, of the order of 30 μm.

4. DESCRIPTION OF THE EXPERIMENTAL SETUP

4.1. Normal Diffusivity Measurement (Flash Method)

Tests were performed both with a setup assembled at our institute and with the apparatus available at LEMTA in Nancy, France. Our setup is shown in Fig. 4. A YAG laser pulse of nearly 0.6-ms duration and 0.5 J is projected over the full 10-mm-diameter face of the sample. The back temperature history (peak temperature elevations were typically between 5 and 10 C) is monitored by an InSb infrared detector, germanium filtered to select the 2- to 5.5-μm spectral band. The LEMTA apparatus uses nearly 3-ms-long, 1500-J light pulses produced by arc-discharge tubes, which were projected over the 20-mm-diameter samples. The temperature was sensed by contacting the sample back face with high-thermoelectric power ($360\ \mu V \cdot C^{-1}$ at 20 C) p- and n-doped Bi_2Te_3 plates separately applied on the sample surface. Electrical conduction takes place through the sample in the case of tungsten, while in the case of zirconia a thin silver coating is applied to the back of the sample.

4.2. Lateral Diffusivity Measurements (Strip Monitoring Method)

The method described in Section 2.2 requires temperature measurements simultaneously at two positions along the strip. In practice, it is difficult to obtain identical sensors and to estimate precisely the positions of, and thus the distance between, the centers of gravity of the sensed areas. We thus used a single infrared temperature sensor pointed to one of the two positions to acquire the first signal, then we displaced micrometrically the sensor along the strip to the other position and repeated the measurement to acquire the second signal (Fig. 5). Although heat flows

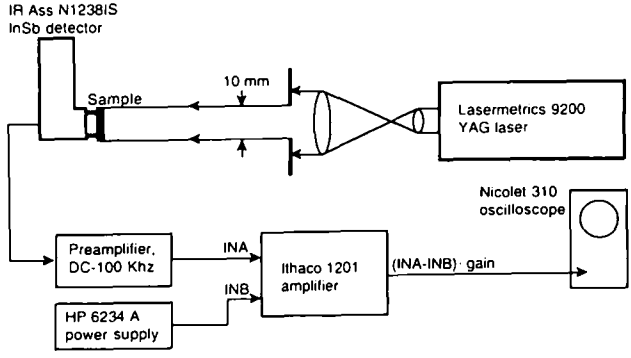

Fig. 4. Setup used at our institute for the face-normal thermal diffusivity measurements.

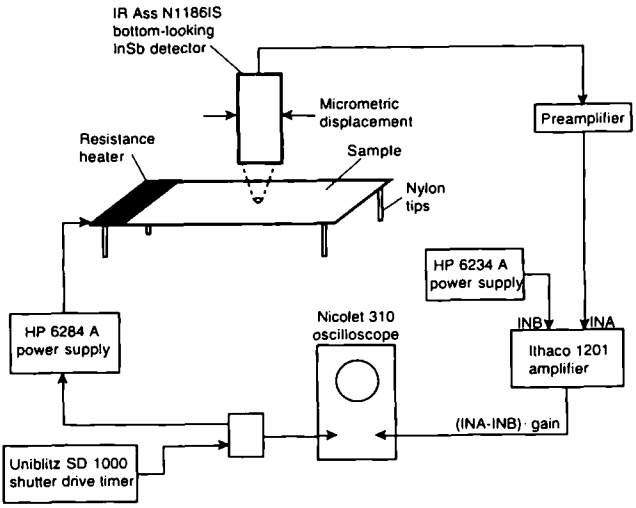

Fig. 5. Setup used at our institute for the face-parallel thermal diffusivity measurements.

may be different in the two measurements due to ambient temperature and surface loss fluctuations, this approach has the advantage of providing an exact absolute evaluation of the distance l between the sensed spots.

Heat injection is performed through a Minco heating resistance lap-bonded over one end of the strip sample. The temperature sensor is an InSb detector mounted on a micromechanical positioner. Peak temperature elevations were typically between 30 and 40°C, except for the case of the 5-s heating time on zirconia, where the peak temperature was of the order of 3°C. A programmable timer triggers the heater and provides a synchronization signal giving the initial time reference. The setup is cloth-protected against ambient temperature fluctuations.

5. RESULTS

5.1. Preliminary Verification on an Isotropic Material (Stainless Steel)

To test the validity of our thermal anisotropy measurements, we first measured the normal and lateral thermal diffusivity of a 1.515-mm-thick stainless-steel plate. The normal diffusivity was measured with our institute's setup on a 10-mm-diameter sample, while the lateral diffusivity was measured on a $300 \times 14\text{-mm}^2$ strip of the same material, using the strip monitoring method described above with a heating time of 80 s and a

Table I. Test Measurements on Stainless Steel

Test No.	Thermal diffusivity (10^{-6} m$^2 \cdot$ s^{-1})	
	Normal	Lateral
1	3.70	3.91
2	3.67	3.52
3	3.67	3.80
4	3.71	3.65
Mean	3.69	3.72
SD, σ	0.02	0.15

distance of 10 mm between the two monitored spots. The p interval used for our evaluation was 0.04–0.06. The results are given in Table I.

We have thus verified that our two methods for the measurement of the normal and lateral thermal diffusivity give the same results to within a few percent. It will also be noticed that the standard deviation for the lateral diffusivity measurements is eight times larger than for the normal diffusivity.

5.2. Zirconia Samples

5.2.1. Normal Diffusivity (Flash Method)

The normal diffusivity was evaluated both with the apparatus available at LEMTA and with our institute's setup. Measurements at LEMTA were performed on a sample 20 mm in diameter and 0.81 mm in thickness. The sample back face was covered with a thin silver coating to provide electrical conduction for the Bi_2Te_3 detector. Table II gives the results obtained on 4 repeated measurement runs.

Table II. Results Obtained for Zirconia, Normal Diffusivity, with the LEMTA Setup

Test No.	t_{12} (ms)	t_{56} (ms)	Normal thermal Diffusivity (10^{-7} m$^2 \cdot$ s^{-1})
1	159	297	5.90
2	153.5	280	5.97
3	150	270	6.02
4	151	271	5.96
Mean, $\bar{a}$			5.96
SD, σ			$0.043 = 0.7\%\ \bar{a}$

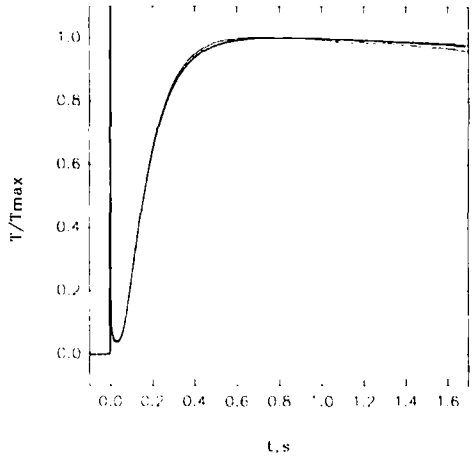

Fig. 6. Plasma-sprayed zirconia: experimental thermograms for the measurement of normal thermal diffusivity.

Table III. Results Obtained for Zirconia, Normal Diffusivity, with the IMI Setup

Test No.	$t_{1/2}$ (ms)	$t_{5/6}$ (ms)	Normal thermal Diffusivity (10^{-7} m^2·s^{-1})
	Sample No. 1 (thickness $e = 0.792$ mm)		
1	159.5	290	5.47
2	159.5	290.5	5.48
3	159	290	5.51
4	158.5	284	5.42
Mean, $\bar{a}$			5.47
SD, σ			$0.03 = 0.6\%\ \bar{a}$
	Sample No. 2 (thickness $e = 0.730$ mm)		
1	130	237	5.72
2	132.5	237.5	5.51
3	130.5	237	5.67
4	133	238.5	5.49
Mean, $\bar{a}$			5.60
SD, σ			$0.1 = 1.8\%\ \bar{a}$

At our institute, two similar samples of 10-mm diameter were tested. As zirconia is translucent, particularly in the infrared detector band, thin gold–palladium coatings were sputtered on both faces at a rate of 5 nm · min $^{-1}$. We found by repeating tests with increasing coating thickness that a gold–palladium thickness of 0.15 μm made the sample opaque and stabilized the thermal response. The experimental signals are shown in Fig. 6, and the corresponding results are given in Table III. We mention for reference that without the gold–palladium coating, the following results were obtained: Sample 1, $t_{1,2} = 89$ ms and $t_{5,6} = 229$ ms; and Sample 2, $t_{1,2} = 68.5$ ms and $t_{5,6} = 183.5$ ms.

5.2.2. Lateral Diffusivity (Strip Monitoring Method)

For the lateral thermal diffusivity measurements, a zirconia band of $100 \times 12\text{-mm}^2$ size and nearly 0.75-mm thickness was produced. Two configurations were chosen for the tests.

- In the first configuration, a heating time of 5 s was chosen, with a distance of 2 mm between the sensing points. We performed four tests (without moving the sample between each test), which gave the signals shown in Fig. 7. The Laplace-variable interval was chosen as 0.158–0.25. The corresponding diffusivities are given in Table IV.

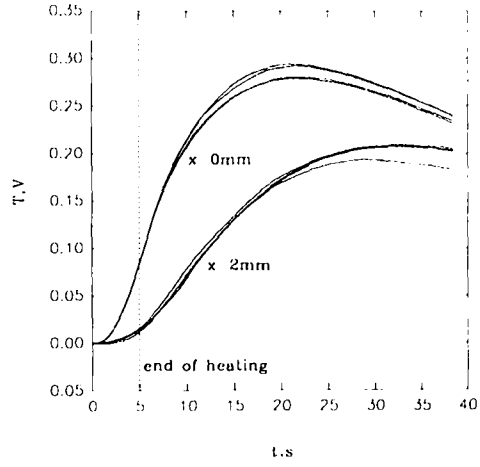

Fig. 7. Plasma-sprayed zirconia: experimental thermograms for the measurement of lateral thermal diffusivity: 5-s heating; $l = 2$ mm.

Table IV. Results for Zirconia, Lateral Diffusivity

Test No.	Lateral thermal diffusivity (10^{-7} m$^2 \cdot$ s^{-1})	
	1st configuration	2nd configuration
1	5.95	8.77
2	8.34	7.23
3	7.47	7.06
4	7.48	6.92
Mean, $\bar{a}$	7.3	7.5
SD, σ	0.9	0.7

- In the second configuration, the heating time was 60 s and the distance between the sensing points 5 mm. The signals are shown in Fig. 8. The diffusivities, as obtained with a 0.04–0.16 Laplace-variable interval, are shown in Table IV.

For reference, a third configuration was also tested, for which the sensitivity, according to the theory, is inadequate: The heating time was 60 s; the distance between sensing points, 2 mm (one should thus have $p > 0.125$); and the Laplace-variable interval, 0.04–0.16. The results were $\bar{a} = 5.7 \cdot 10^{-7}$ m$^2 \cdot$ s^{-1} and $\sigma = 0.8 \cdot 10^{-8}$ m$^2 \cdot$ s^{-1}.

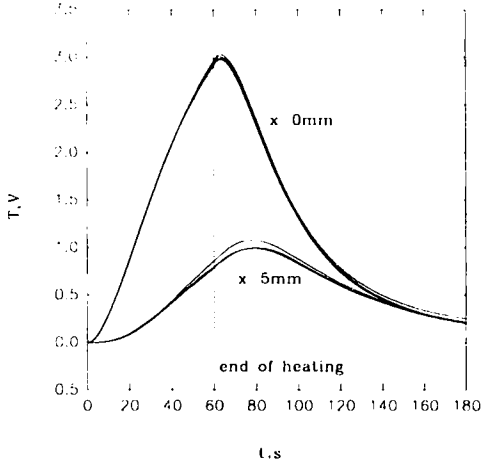

Fig. 8. Plasma-sprayed zirconia: experimental thermograms for the measurement of lateral thermal diffusivity: 60-s heating; $l = 5$ mm.

Table V. Results for 0.82-mm-Thick Tungsten, Normal Diffusivity, with the LEMTA Setup

Test No.	t_{12} (ms)	t_{56} (ms)	Normal thermal Diffusivity (10^{-6} m$^2 \cdot$ s^{-1})
1	21.85	36.90	3.89
2	21.95	37.20	3.89

5.3. Tungsten Samples: Thickness, ≈ 0.8 mm

5.3.1. Normal Diffusivity (Flash Method)

The first set of tungsten samples, of a thickness close to 0.8 mm, was tested for the face-normal thermal diffusivity by using the flash setups available both at our institute and at LEMTA. The LEMTA tests were performed on a 0.82-mm-thick, 20-mm-diameter sample. The results are given in Table V.

At our institute, 2 samples of 10-mm diameter and slightly different thicknesses (see below) gave the experimental signals shown in Fig. 9 and the results given in Table VI.

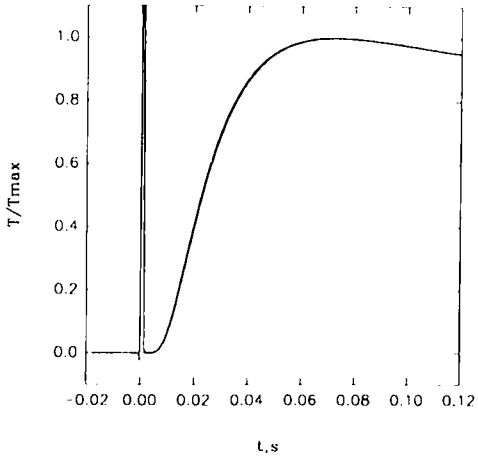

Fig. 9. Plasma-sprayed tungsten: experimental thermograms for the measurement of normal thermal diffusivity (first projected sample: $e \cong 0.8$ mm).

Table VI. Results for Nearly 0.8-mm-Thick Tungsten, Normal Diffusivity, with the IMI Setup

Test No.	$t_{1/2}$ (ms)	$t_{5/6}$ (ms)	Normal thermal Diffusivity (10^{-6} m^2·s^{-1})
	Sample No. 1 (thickness $e = 0.791$ mm)		
1	22.75	37.55	3.35
2	22.90	37.70	3.32
3	22.55	37.20	3.38
4	22.90	37.65	3.31
Mean, $\bar{a}$			3.34
SD, σ			$0.03 = 0.8\%\ \bar{a}$
	Sample No. 2 (thickness $e = 0.830$ mm)		
1	21.35	35.65	4.01
2	21.35	35.70	4.02
3	21.60	36.25	3.99
4	21.35	35.75	4.03
Mean, $\bar{a}$			4.01
SD, σ			$0.02 = 0.4\%\ \bar{a}$

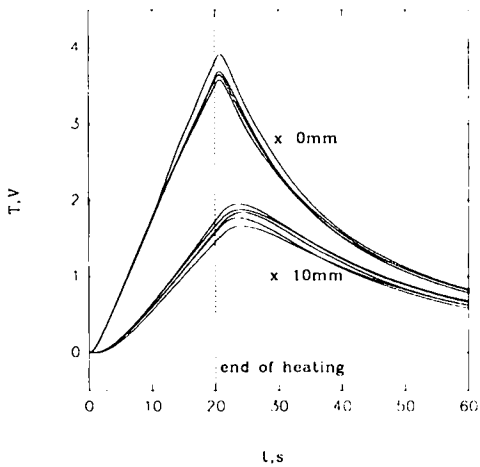

Fig. 10. Plasma-sprayed tungsten: experimental thermograms for the measurement of lateral thermal diffusivity: 20-s heating; $l = 10$ mm. First sample ($e \cong 0.8$ mm).

Table VII. Results for Nearly 0.8-mm-Thick Tungsten, Lateral Diffusivity

Test No.	Lateral thermal diffusivity (10^{-6} m$^2 \cdot$s^{-1})	
	1st configuration	2nd configuration
1	22.2	19.0
2	19.9	18.3
3	19.6	18.6
4	19.3	22.7
5	21.4	19.7
Mean, $\bar{a}$	20.5	19.7
SD, σ	1.1	1.6

5.3.2. *Lateral Diffusivity (Strip Monitoring Method)*

The tungsten strip sample, of 100×12-mm^2 size and nearly 0.8-mm thickness, was heated for 20 s and the distance between sensing points was 10 mm. The corresponding experimental signals are shown in Fig. 10. This was the preferred configuration. For reference, we also tested a second configuration for which the theory gives a worst sensitivity: a distance between sensing points of 5 mm, for which one should have $p > 0.6$. In both cases, we adopted a Laplace-variable interval of 0.15–0.25. The results are given in Table VII.

Table VIII. Results for Nearly 1.3-mm-Thick Tungsten, Normal Diffusivity, with the LEMTA Setup

Test No.	t_{12} (ms)	t_{56} (ms)	Normal thermal diffusivity (10^{-6} m$^2 \cdot$s^{-1})
	Sample No. 1 (thickness $e = 1.314$ mm)		
1	40.0	67.3	5.43
2	41.4	70.0	5.28
Mean, $\bar{a}$			5.36
SD, σ			$0.08 = 1.4\%\ \bar{a}$
	Sample No. 2 (thickness $e = 1.274$ mm)		
1	37.8	63.0	5.32
2	38.95	65.4	5.22
Mean, $\bar{a}$			5.27
SD, σ			$0.06 = 0.95\%\ \bar{a}$

Table IX. Results for Nearly 1.3-mm-Thick Tungsten, Normal Diffusivity, with the IMI Setup

Test No.	$t_{1,2}$ (ms)	$t_{5,6}$ (ms)	Normal thermal diffusivity (10^{-6} m^2·s^{-1})
	Sample No. 3 (thickness $e = 1.293$ mm)		
1	35.8	58.0	5.51
2	35.9	58.2	5.50
3	35.8	58.2	5.54
4	36.1	58.6	5.48
5	36.0	58.5	5.51
Mean, $\bar{a}$			5.51
SD, σ			$0.02 = 0.35\%\ \bar{a}$
	Sample No. 4 (thickness $e = 1.394$ mm)		
1	41.9	67.1	5.35
2	41.9	67.1	5.35
3	41.7	66.6	5.35
4	41.7	66.9	5.40
5	41.5	66.5	5.41
Mean, $\bar{a}$			5.37
SD, σ			$0.03 = 0.5\%\ \bar{a}$

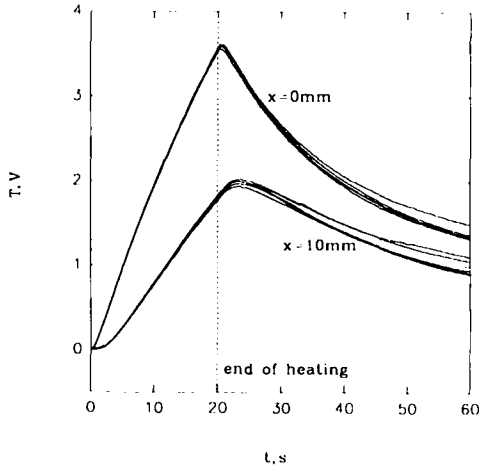

Fig. 11. Plasma-sprayed tungsten: experimental thermograms for the measurement of the lateral thermal diffusivity: 20-s heating; $l = 10$ mm. Second sample ($e \cong 1.3$ mm).

Table X. Results for Nearly 1.3-mm-Thick Tungsten, Lateral Diffusivity

Test No.	Lateral thermal diffusivity 1st configuration (10^{-6} m$^2 \cdot$s^{-1})
1	23.7
2	24.5
3	26.9
4	21.2
5	23.1
Mean, $\bar{a}$	23.9
SD, σ	1.9

5.4. Tungsten Samples: Thickness, $\approx$ 1.3 mm

5.4.1. Normal Diffusivity (Flash Method)

The second set of tungsten samples, of a thickness close to 1.3 mm, was tested for the face-normal thermal diffusivity, again using the flash setups available both at our institute and at LEMTA. The LEMTA tests were performed on two samples, both of 20-mm diameter and thicknesses given below. Table VIII contains the results.

The IMI tests were performed on two 10-mm-diameter samples. The diffusivities are in Table IX.

5.4.2. Lateral Diffusivity (Strip Monitoring Method)

The tungsten strip sample, of 100×12-mm^2 size and nearly 1.3-mm thickness, was heated for 20 s, with a distance between sensing points of 10 mm. The corresponding experimental signals are shown in Fig. 11. The

Table XI. Average Thermal Diffusivities Obtained in the Different Cases

Sample type	Avg. normal thermal diffusivity (m$^2 \cdot$s^{-1})		Avg. lateral thermal diffusivity (m$^2 \cdot$s^{-1})
	LEMTA setup	IMI setup	
Zirconia	5.96×10^{-7} (without Au–Pd)	1: 5.47×10^{-7} 2: 5.60×10^{-7} (with Au–Pd)	1: $(7.3 \pm 0.9)\ 10^{-7}$ 2: $(7.5 \pm 0.7)\ 10^{-7}$
Tungsten $e \approx 0.8$ mm	3.89×10^{-6} (thickness, 0.82 mm)	3.34×10^{-6} (0.79 mm) and $4.01 \cdot 10^{-6}$ (0.83 mm)	$(20.5 \pm 1)\ 10^{-6}$
$e \approx 1.3$ mm	1: 5.36×10^{-6} 2: 5.27×10^{-6}	3: 5.51×10^{-6} 4: 5.37×10^{-6}	$(23.9 \pm 2)\ 10^{-6}$

lateral thermal diffusivities as computed with a p interval of 0.15–0.315 are given in Table X.

5.5. Summary of the Thermal Diffusivity Measurements

Finally, we summarize in Table XI the average diffusivities obtained in the different cases.

5.5.1. Thermal Anisotropy Calculation

By taking the ratio of the above lateral and normal thermal diffusivities, one obtains the following anisotropy values and maximal deviations: zirconia, 1.3 ± 0.2; tungsten, 0.8 mm thick, 5.5 ± 0.6; and tungsten, 1.3 mm thick, 4.4 ± 0.5.

6. DISCUSSION AND CONCLUSION

The results obtained show that the thermal anisotropy of plasma-sprayed tungsten coatings is much higher than that of zirconia coatings. This was expected, as the influence of the particle-to-particle thermal resistance is higher for a high thermal conductivity material, such as tungsten, than for zirconia. It should be recalled [17] that the normal thermal conductivity in plasma-sprayed tungsten coatings is due mainly to particle-to-particle interfaces.

The normal thermal diffusivity of tungsten coatings appears to be significantly correlated with their thickness. This is probably due to the increase in the coating temperature during spraying: Thicker coatings heat up to higher temperatures during spraying, resulting in a lower particle-to-particle thermal resistance. The lateral thermal diffusivity being less affected by the particle-to-particle thermal resistance, the net result is a higher anisotropy for thinner coatings.

There appears to be a significant difference in the normal thermal diffusivity values obtained at LEMTA with zirconia samples having no Au–Pd coating compared to the IMI results obtained on samples with thin opaque coatings. This is due, at least in part, to optical penetration for the flash light. The results suggest a value of the order of 30 μm for such an optical penetration depth. This is in rough agreement with spectral transmittance tests we performed in the near-IR region on thin plasma-sprayed zirconia coatings. For these reasons, we have disregarded the bare-sample results in our anisotropy calculations.

The reproducibility of our normal thermal diffusivity measurements appears to be satisfactory, differences from sample to sample being due probably, in part at least, to structural differences within the different

samples. Systematic errors due to surface losses should be avoided by our data processing method.

Results obtained for the lateral thermal diffusivity were less reproducible, probably because of the surface loss fluctuations both within each signal and relative to each other. The overall precision was, however, improved by averaging over a number of tests, while systematic errors related to bad evaluations of the distance between the sensing spots were avoided with our micrometric displacement method.

ACKNOWLEDGMENTS

The authors are grateful to Sylvain Bélanger of NRC-IMI for technical assistance in the preparation of the plasma-sprayed samples. Facilities for a number of thermal measurements were kindly provided by the LEMTA laboratory in Nancy, France.

REFERENCES

1. R. MacPherson, *Thin Solid Films* **83**:297 (1981).
2. R. MacPherson, *Thin Solid Films* **112**:89 (1984).
3. L. Pawlowski, D. Lombard, and P. Fauchais, *J. Vac. Sci. Technol. A* **3**:2494 (1985).
4. P. Cielo and S. Dallaire, *J. Mater. Eng.* **9**:71 (1987).
5. L. C. Aamodt, J. W. Maclachlan Spicer, and J. C. Murphy, in *Photoacoustic and Photothermal Phenomena 2*, J. C. Murphy, J. W. Maclaclan Spicer, L. Aamodt, and B. S. H. Royce, eds. (Springer-Verlag, Berlin, 1990), p. 59.
6. M. F. Elchinger, C. Martin, and P. Fauchais, *Rev. Int. Hautes Temp. Refract.* **16**:317 (1979).
7. R. Brandt, *High Temp.-High Press.* **13**:79 (1981).
8. P. Cielo, *J. Appl. Phys.* **56**:230 (1984).
9. L. Pawlowski, D. Lombard, F. Turenne, F. Kassabji, and P. Fauchais, *High Temp.-High Press.* **17**:611 (1985).
10. E. P. Roth and M. F. Smith, *Int. J. Thermophys.* **7**:455 (1986).
11. J. W. Maclachlan, L. C. Aamodt, and J. C. Murphy, *Ceram. Eng. Sci. Proc.* **9**:1181 (1988).
12. H. P. R. Frederikse, X. T. Ying, and A. Feldman, *Mater. Res. Soc. Symp. Proc.* **142**:289 (1989).
13. T. Velinov, B. Gergov, and K. Bransalov, *Rev. Phys. Appl.* **25**:817 (1990).
14. S. K. Lau, D. P. Almond, and P. M. Patel, *J. Phys. D Appl. Phys.* **24**:428 (1991).
15. L. D. Favro, T. Ahmed, D. Crowter, H. J. Jin, P. K. Kuo, R. L. Thomas, and X. Wang, *Proc. SPIE* **1467**:290 (1991).
16. A. Mandelis, S. B. Peralta, and J. Thoen, *J. Appl. Phys.* **70**:1761 (1991).
17. C. Moreau, P. Fargier-Richard, R. G. Saint-Jacques, and P. Cielo, in *Proc. Int. Conf. Metallurg. Coat. Thin Films*, San Diego, March (1993).
18. S. W. Kim and R. E. Taylor, *Int. J. Thermophys.* **14**:135 (1993).
19. B. K. Bein, in *Progress in Photothermal and Photoacoustic Science 2*, A. Mandelis, ed. (Prentice-Hall, Toronto, 1993).
20. K. Tani, H. Nakahira, K. Miyajima, and Y. Harada, *Mater. Trans. Jpn. Inst. Metals* **33**:618 (1992).

21. R. E. Taylor, *High Temp.-High Press.* **11**:43 (1979).
22. I. Hatta, *Int. J. Thermophys.* **11**:293 (1990).
23. A. B. Donaldson and R. E. Taylor, *J. Appl. Phys.* **46**:4584 (1975).
24. F. I. Chu, R. E. Taylor, and A. B. Donaldson, *J. Appl. Phys.* **51**:336 (1980).
25. M. Lachi and A. Degiovanni, *J. Phys. III Fr.* **1**:2027 (1991).
26. J. C. Krapez, P. Cielo, X. Maldague, and L. A. Utracki, *Polym. Comp.* **8**:396 (1987).
27. M. J. Folkes and H. A. Potts, *Plast. Rubb. Proc. Appl.* **10**:79 (1988).
28. P. Cielo, L. A. Utracki, and M. Lamontagne, *Can. J. Phys.* **64**:1172 (1986).
29. F. Enguehard, D. Boscher, A. Déom, and D. Balageas, *Mater. Sci. Eng.* **B5**:127 (1990).
30. G. Lu and W. T. Swann, *Appl. Phys. Lett.* **59**:1556 (1991).
31. H. Shibata, H. Ohta, and Y. Waseda, *Mater. Jpn. Inst. Metals* **32**:837 (1991).
32. J. E. Graebner, S. Jin, G. W. Kammlott, B. Bacon, L. Seibles, and W. Banholzer, *J. Appl. Phys.* **71**:5353 (1992).
33. D. Hadisaroyo, J. C. Batsale, and A. Degiovanni, *J. Phys. III Fr.* **2**:111 (1992).
34. W. J. Parker, R. J. Jenkins, G. P. Butler, and G. L. Abbott, *J. Appl. Phys.* **32**:1979 (1961).
35. A. Degiovanni, *Rev. Gen. Therm. Fr.* **185**:417 (1977).